

Insight into Improving Energy Efficiency of Electrochemical CO₂ Reduction to Formate in Divided H-type Cell

Rui Zhang, Luyu Shao, Jiajia Wu, Yajin Chen, Weixin Lv*, Wei Wang*

School of Chemistry and Chemical Engineering, Yancheng Institute of Technology, Yancheng 224051, China

*E-mail: weixin841230@126.com (W.X. Lv), wangw@ycit.edu.cn (W. Wang).

Received: 2 November 2020 / Accepted: 23 December 2020 / Published: 31 January 2021

The conversion of carbon dioxide (CO₂) into formate by the intermittent generation of renewable energy is of great interest for many applications. Most studies have so far focused on how to improve the faradaic efficiency but ignored the importance of energy efficiency. In this study, the electrochemical reduction of CO₂ (ERC) was carried out in a divided H-type electrolyzer. The improvement of energy efficiency was studied in the context of three aspects: (1) contrasting the cathodic catalysts, *i.e.*, traditional Sn foil with highly active nano-Bi (produced in situ by reduction from nano-Bi₂O₃), (2) comparing anodic catalysts, *i.e.*, traditional Pt plate and the as-prepared Ir/C, and (3) contrasting anodic electrolytes, *i.e.*, aqueous solutions of KHCO₃ and KOH. The energy efficiency of the ERC to formate can reach 38.2% with the r-Bi₂O₃ cathodic catalyst, and Ir/C anodic catalyst were used in 1.0 M KOH anolyte, at a low cell potential (2.06 V). This work concluded that KOH anolyte is more suitable for the ERC to formate. Furthermore, the method of calculating the energy efficiency for the ERC to formate was also systematically reviewed.

Keywords: cathodic catalyst, anodic catalyst, anolyte, energy efficiency, H-type electrolyzer

1. INTRODUCTION

Electrochemical reduction of CO₂ (ERC) is a potential solution to reduce CO₂ emissions and alleviate power fluctuation of renewable energy sources [1]. It is becoming an increasingly important method due to its ease of operation combined with the advantages of using renewable energy and diversity of add-valued organic products [2]. Numerous studies suggest high faradaic efficiency for the ERC to formate [3, 4]. However, to use ERC as an energy storage strategy, the energy efficiency of the reaction process should also be optimized [5].

At present, energy efficiency can be enhanced by improving the performance of both cathodic and anodic catalysts to decrease the overpotentials of the corresponding electrode. Many materials have

been reported as the cathodic catalysts for the ERC to formate with high faradaic efficiency [6-11]. Among them, the Bi-based cathodic catalyst is promising because of its low overpotential and high stability [12-15]. Pt is usually used as the anodic catalyst for ERC [16-18], but it possesses high overpotential and low activity for the oxygen evolution reaction (OER) [5]. By comparison, Ir-based catalysts are stable and have good catalytic performances towards OER [19, 20]. Yu *et al.* prepared a nano-sized $\text{IrO}_x/\text{Nafion}$ composite catalyst for OER with good activity and high stability under electrolysis for about 4500 h [21].

To industrialize the process of the ERC to formate, typically, a double-compartment electrolytic cell is used to prevent the resulting formate from being oxidized at the anode [22]. Zhao *et al.* reported that the energy efficiency of the ERC to formate, using Pt anode, was only 27% in a double-compartment electrolytic cell, in which the anolyte and catholyte were both aqueous KHCO_3 solutions [23]. The aqueous KHCO_3 solution is generally employed as both the anolyte and catholyte for ERC [12, 24, 25]. Using a KHCO_3 solution as catholyte can provide high faradaic efficiency [26]. While, KOH solutions also can be used as the anolyte [14, 27, 28], the advantages or reason for the choice of either anolyte has not been clearly stated in literature.

At present, there are few reports of systematic investigations on the energy efficiency of the ERC to formate. In this work, the ERC to formate was performed in a divided H-type electrolytic cell. We employed Bi-based cathodic and Ir-based anodic high activity catalysts in order to increase energy efficiency. The effects of the KOH and KHCO_3 anolytes on energy efficiency, and their differences, have been studied and discussed. The method for estimating the energy efficiency for the ERC to formate was also systematically reviewed.

2. EXPERIMENTAL

2.1 Preparation of cathodic catalyst modified GCE

2 mmol $\text{Bi}(\text{NO}_3)_3 \cdot 5\text{H}_2\text{O}$ and 1.5 mmol citric acid were dissolved into 10 mL of 1 M HNO_3 solution. With NaOH, the pH was adjusted to 4, the mixed solution was transferred into a Teflon-lined autoclave and kept at 180 °C for 24 h. The as-prepared white precursor was retrieved by centrifugation, washed several times with deionized water and absolute ethanol, and then vacuum-dried at 60 °C for 5 h. Finally, the dried sample was calcined under air atmosphere at 500 °C for 3 h to obtain the light-yellow Bi_2O_3 .

40 mg of the as-prepared Bi_2O_3 was first dissolved in 1 mL of ethanol, to which 0.1 mL of a 5 wt% Nafion solution was added, and was subsequently sonicated for 20 min. Afterwards, 10 μL of the solution prepared above was pipetted onto a freshly polished L-style glass carbon electrode (GCE, diameter 5 mm) and dried in air. The Bi_2O_3 deposited on the GCE was reduced at -1.5 V vs. Ag/AgCl in a 0.1 M KHCO_3 aqueous solution for 10 min. The reduced Bi_2O_3 modified GCE, denoted as r- $\text{Bi}_2\text{O}_3/\text{GCE}$, was prepared and then dried in air for 10 min before further experiments.

2.2 Preparation of anodic catalyst modified GCE

N-doped carbon nanotubes (CN_xNTs) were synthesized from an n-propylamine precursor with Co_{0.1}Mg_{0.9}MoO₄ catalyst by chemical vapor deposition. 30 mg of CN_xNTs powder was dispersed in an ethanol/water mixture (volume ratio: 9:1) and sonicated for 1 h. The above solution was mixed with H₂IrCl₆ under stirring at 25 °C for 2 h and then stirred at 80 °C for 6 h. Then, the mixture was placed in an autoclave and held at 150 °C for 4 h. Finally, the product was centrifuged, washed with ethanol/water solution, and vacuum-dried at 80 °C for 10 h. The catalyst with 20 wt% of Ir was obtained and named as Ir/C in the following.

Briefly, 3 mg of the Ir/C catalyst was ultrasonically dispersed in 200 μL of ethanol and 6 μL of Nafion solution (5 wt%) for 30 min. Afterwards, 10 μL of the catalyst ink was deposited on the freshly polished L-style GCE (diameter 5 mm) and dried in air.

2.3 Electrochemical experiments

The electrochemical experiments were carried out on a CHI660E electrochemical workstation (Shanghai Chenhua Instruments Co., Ltd., China) in a divided H-type two-compartment glass cell with 50 mL electrolyte per chamber. The two chambers were separated by a proton exchange membrane (Nafion 117) to allow ionic conductivity and minimize the anodic oxidation of formic acid. The cathodic electrolyte was CO₂-saturated 0.1 M KHCO₃ aqueous solution (pH=7). The anodic electrolytes used in this study are either 0.1 M KHCO₃, 0.1 M KOH, or 1.0 M KOH aqueous solutions.

Linear sweep voltammetry (LSV) was performed in a three-electrode system, where an Ag/AgCl electrode (saturated KCl) was acted as the reference electrode. The cathode was either an Sn foil (0.2 cm²) or the synthesized r-Bi₂O₃/GCE, while the anode was a Pt plate (0.2 cm²) or the Ir/C modified GCE. The cathodic and anodic potential scan rates were all set at 5 mV s⁻¹.

The cell potential between the cathode and anode was measured by a digital multimeter (VICTOR VC9808⁺). The constant cell potential electrolysis was performed for 2 h at the cell potential in the two-electrode system (cathode||anode system) without a reference electrode. The cathodic electrolyte was continuously sparged with CO₂ during the electrolysis process.

2.4 Analysis and calculations

The morphology and structure of the Bi₂O₃ sample were examined with a scanning electron microscope (SEM, Hitachi S-4800) and X-ray diffraction (XRD, Bruker D8). The morphology and surface element content of the Ir/C catalyst were examined with transmission electron microscopy (TEM, JEOL-2100) and X-ray photoelectron spectroscopy (XPS, VG ESCALAB 250). The formate species in the electrolyte were directly analyzed by ion chromatography (Dionex ICS-5000⁺).

The faradaic efficiency (*FE*) and energy efficiency (*EE*) of the ERC to formate can be calculated by the following equations:

$$FE = 2nF/Q \quad (1)$$

$$EE = |E^0| \times FE / \text{Cell potential} \quad (2)$$

where n is the number of moles of the generated formate which can be calculated from the data of ion chromatography; F is 96485 C mol^{-1} ; Q is the electrical charge passed through the system during the electrolysis; and $|E^0|$ is the absolute value of the equilibrium cell potential for the formate product.

3. RESULTS AND DISCUSSION

3.1 Effect of cathodic catalyst

The SEM image of the synthesized Bi_2O_3 is presented in Figure 1A. It can be seen that the sample is composed of nanoparticles with an average diameter of around 500 nm. The XRD pattern in Figure 1B shows that all the peaks for the sample could be readily indexed to the monoclinic $\alpha\text{-Bi}_2\text{O}_3$, which agrees well with the standard XRD patterns of Bi_2O_3 (JCPDS card No. 71-2274).

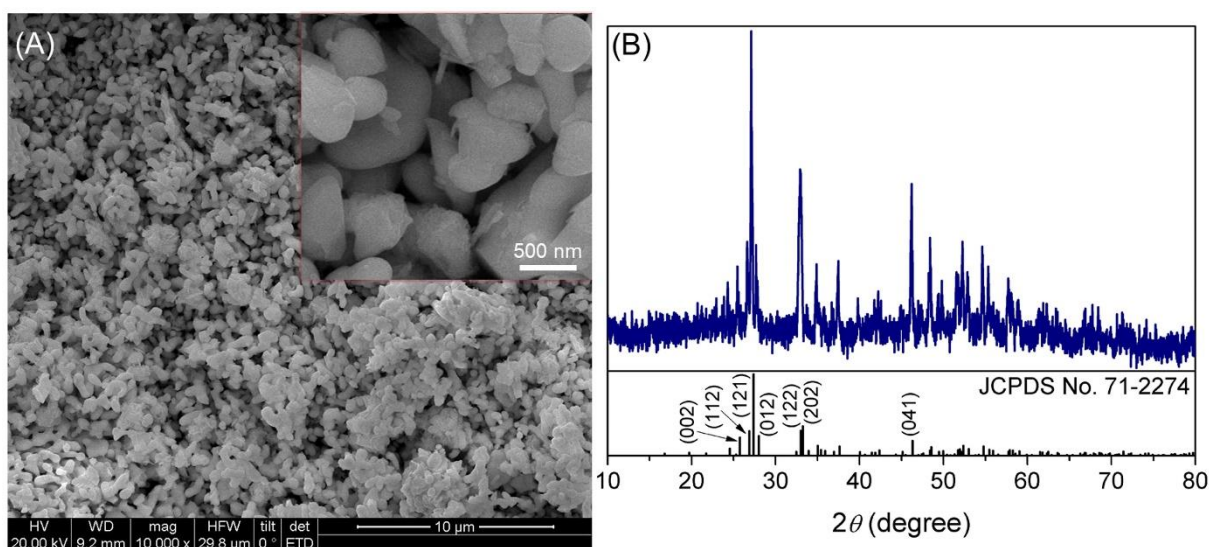


Figure 1. A, SEM image of Bi_2O_3 (the insert image shows the magnified SEM image of Bi_2O_3). B, XRD pattern of Bi_2O_3 .

The electrochemical reduction of Bi_2O_3 to $\text{r-Bi}_2\text{O}_3$ was achieved at $-1.5 \text{ V vs. Ag/AgCl}$ within 10 min. As shown in Figure 2, the current stabilized after 6 min of electrolysis. In the inset of Figure 2, the color of Bi_2O_3 is shown to be light yellow, while that of $\text{r-Bi}_2\text{O}_3$ is black. Therefore, the reduction of oxidized Bi to metal Bi can be detected through the change in color and the current-time curve.

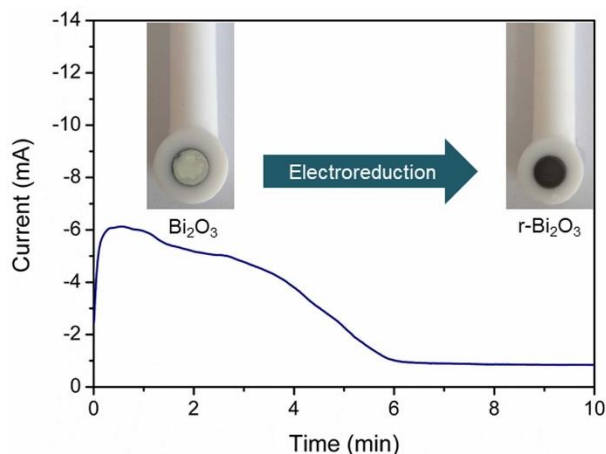


Figure 2. Current versus time during the reduction of Bi_2O_3 to $\text{r-Bi}_2\text{O}_3$ at -1.5 V vs. Ag/AgCl. The insert images show the photographs of $\text{Bi}_2\text{O}_3/\text{GCE}$ and $\text{r-Bi}_2\text{O}_3/\text{GCE}$.

Figure 3 depicts the LSV curves obtained from $\text{r-Bi}_2\text{O}_3/\text{GCE}$ and the Sn foil in CO_2 -saturated 0.1 M KHCO_3 catholyte and 0.1 M KHCO_3 anolyte. Compared to the Sn foil, an obvious increase of the current density can be seen on the cathodic end for $\text{r-Bi}_2\text{O}_3/\text{GCE}$. In addition, the initial potential of $\text{r-Bi}_2\text{O}_3/\text{GCE}$ is lower than that of the Sn foil. These results indicated the strong catalytic activity of $\text{r-Bi}_2\text{O}_3$ towards ERC when compared to Sn.

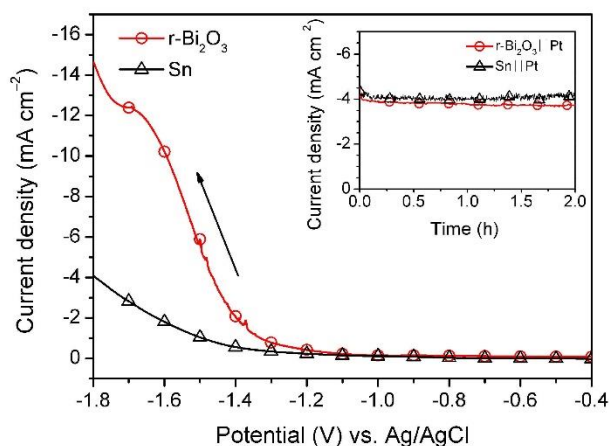
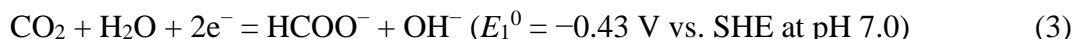


Figure 3. LSV curves recorded on $\text{r-Bi}_2\text{O}_3/\text{GCE}$ and Sn electrode in CO_2 -saturated 0.1 M KHCO_3 catholyte and 0.1 M KHCO_3 anolyte at 5 mV s^{-1} (the counter electrode is the Pt electrode). Inset picture shows the curves of current density versus time during ERC using $\text{r-Bi}_2\text{O}_3 \parallel \text{Pt}$ system at 3.30 V and $\text{Sn} \parallel \text{Pt}$ system at 3.85 V in 0.1 M KHCO_3 catholyte and 0.1 M KHCO_3 anolyte.

According to our previous studies, the optimal cathode electrolysis potentials for the ERC to formate were identified as -1.8 V vs. Ag/AgCl using an Sn-based catalyst and -1.6 V vs. Ag/AgCl using a Bi-based catalyst [8, 29]. In this work, when the electrolysis potentials were set at -1.6 V vs. Ag/AgCl for the $\text{r-Bi}_2\text{O}_3\text{-Pt}$ system and -1.8 V vs. Ag/AgCl for the Sn-Pt system, the corresponding cell potentials were 3.30 and 3.85 V, respectively. The overpotentials (η) of the CO_2 reduction reaction were calculated

as 0.97 V for the r-Bi₂O₃-Pt system and 1.17 V for the Sn-Pt system, according to $\eta = E_1^0 - E(\text{vs. Ag/AgCl}) - 0.20 \text{ V}$, where E_1^0 is the standard electrode potential for the following CO₂ reduction reaction [30]:



Compared to the Sn catalyst, r-Bi₂O₃ can reduce the cathodic overpotential, leading to decreased cell potential. The constant cell potential electrolysis experiments were performed at the corresponding cell potentials of the two-electrode systems (3.30 V for the r-Bi₂O₃ || Pt system and 3.85 V for the Sn || Pt system), and the corresponding results are shown in the inset of Figure 3. The current densities of both systems are constant at around 4 mA cm⁻². The faradaic efficiencies of the ERC to formate in the r-Bi₂O₃ || Pt and Sn || Pt systems were calculated as 95.1% and 73.0%, respectively, by Equation 1. The faradaic efficiencies of the Sn-based catalysts in most literature were around 80% [5, 22, 26, 28], and those of the Bi-based catalysts, were up to 90% [7, 8], which is close to the faradaic efficiency of r-Bi₂O₃ obtained in this work. These studies show that Bi-based catalysts have better application prospects than Sn-based catalysts.

Then, the energy efficiencies of the r-Bi₂O₃ || Pt and Sn || Pt systems were calculated as 33.3% and 21.9%, respectively, by Equation 2. It can be concluded that the r-Bi₂O₃ cathodic catalyst, with a lower cell potential and higher energy efficiency, could lower the electrical energy required to convert CO₂ to formate when compared to the Sn catalyst.

3.2 Effect of anodic catalyst

The total cell potential required for the ERC includes the potentials of both anodic and cathodic processes ($E_{\text{cell}} = E_{\text{anode}} - E_{\text{cathode}}$). Here, the cell potential was reduced by lowering the overpotential of the cathodic reaction; and it can be further decreased if the overpotential of the anodic reaction is lowered. Here, the Ir/C catalyst was prepared and employed as the anodic catalyst in order to decrease the anodic overpotential of OER.

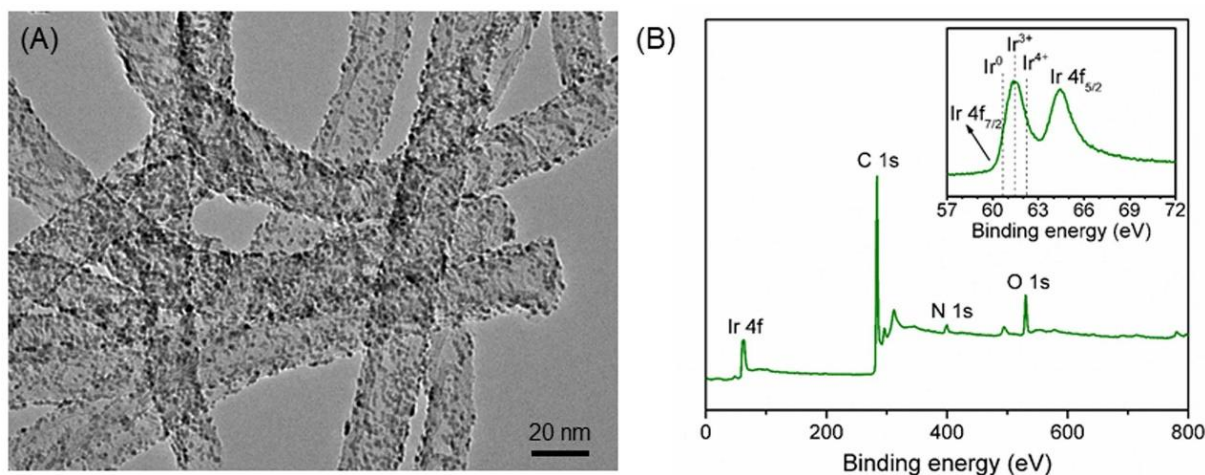


Figure 4. A, TEM image of Ir/C. B, XPS survey spectrum of Ir/C (insert picture is the XPS spectrum of Ir/C in the Ir 4f region).

The morphology of the as-prepared Ir/C catalyst is shown in Figure 4A. The CN_xNTs are around 25 nm in diameter whose surfaces are loaded with IrO₂ particles of 1 nm diameter. In the XPS survey spectrum of the Ir/C catalyst in Figure 4B, the elements C, N, O, and Ir are all present, showing their incorporation into the Ir/C catalyst. The illustration in Figure 4B displays the XPS spectrum of the Ir/C in the Ir 4f region. The binding energies of Ir 4f_{7/2} for Ir⁰, Ir³⁺, and Ir⁴⁺ were recorded as 60.7, 61.5, and 62.2 eV, respectively [31]. From the illustration of Figure 4B, the Ir 4f_{7/2} energy level presents a wide range of binding energies, covering Ir⁰, Ir³⁺, and Ir⁴⁺, indicating that the oxidation states of Ir may consist of 0, +3, and +4.

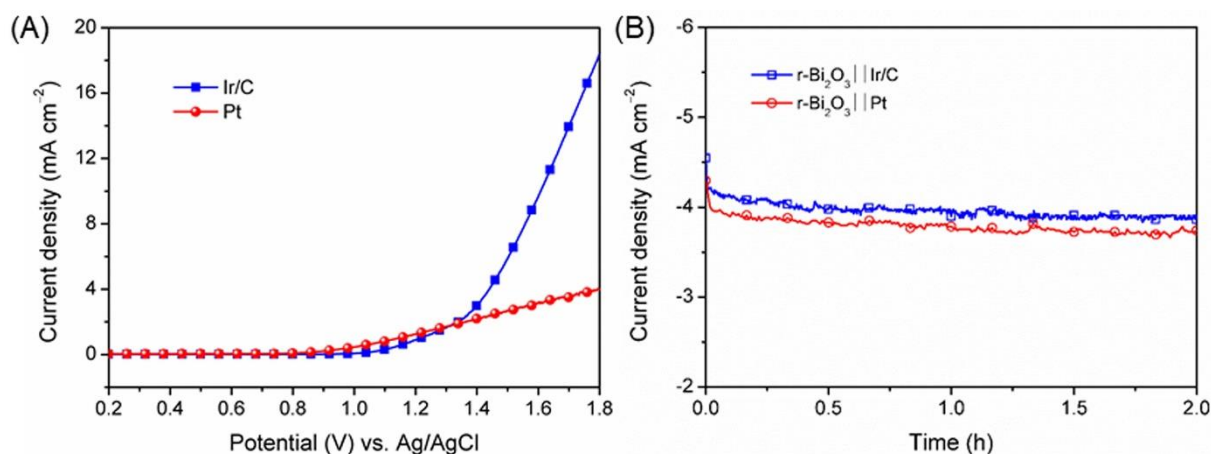


Figure 5. A, LSV curves of OER recorded on Ir/C modified GCE and Pt electrode in CO₂-saturated 0.1 M KHCO₃ catholyte and 0.1 M KHCO₃ anolyte at 5 mV s⁻¹ (the counter electrode is r-Bi₂O₃/GCE). B, Current density versus time during ERC using r-Bi₂O₃ || Ir/C system at 2.83 V and r-Bi₂O₃ || Pt system at 3.30 V in 0.1 M KHCO₃ catholyte and 0.1 M KHCO₃ anolyte.

The OER performances of the Ir/C modified GCE and Pt electrode were evaluated by LSV measurements. As shown in Figure 5A, Ir/C exhibits better OER activity than Pt. When the electrolysis potential was set at -1.6 V vs. Ag/AgCl for the r-Bi₂O₃ || Ir/C system, the corresponding cell potential was recorded as 2.83 V, which was lower than that of the r-Bi₂O₃ || Pt system, indicating that the use of the Ir/C anodic catalyst can indeed reduce the cell potential of the ERC to formate. The constant cell potential electrolysis experiment for the r-Bi₂O₃ || Ir/C system was performed at the cell potential of 2.83 V, and the corresponding result is compared with that of the r-Bi₂O₃ || Pt system in Figure 5B. The faradaic efficiency and energy efficiency of the ERC to formate in the r-Bi₂O₃ || Ir/C system were calculated as 95.3% and 39%, respectively. The energy efficiency of the r-Bi₂O₃ || Ir/C system was higher than that of the r-Bi₂O₃ || Pt system (33.3%), indicating that the Ir/C anodic catalyst can improve the energy efficiency compared to the Pt anodic catalyst.

3.3 Effect of anodic electrolytes

So far, the KHCO₃ aqueous solution has often been used as the anolyte in the double-chamber electrolytic cell for the ERC to formate; however, many OER studies have also been carried out in an

alkaline solution [32, 33]. Here, we studied the impact of the anolytes (KOH and KHCO₃ solutions) on the ERC to formate. Figure 6A shows the LSV curves of the r-Bi₂O₃||Ir/C system in three different anolytes. It can be seen that the highest OER current density is obtained using 1.0 M KOH anolyte. When the electrolysis potential was set at -1.6 V vs. Ag/AgCl for r-Bi₂O₃||Ir/C system, the corresponding cell potentials were recorded as 2.31 V for 0.1 M KOH anolyte and 2.06 V for 1.0 M KOH anolyte, respectively, which were lower than that for 0.1 M KHCO₃ anolyte (2.83 V). Hence, when the KOH solution is used as the anolyte, the cell potential of ERC can be reduced. It also can be concluded that the concentration of the KOH anolyte can affect the cell potential. Electrolysis of the r-Bi₂O₃||Ir/C system, at constant cell potential, in three different anolytes, was performed at the corresponding cell potentials for 2 h. As shown in Figure 6B, the curves of the current densities are nearly identical. The faradaic efficiencies of 0.1 M KHCO₃, 0.1 M KOH, and 1.0 M KOH anolytes for the ERC to formate were calculated as 95.3%, 94.8%, and 95.0%, respectively; and the resulting energy efficiencies were 39.0%, 36.5%, and 38.2%, respectively.

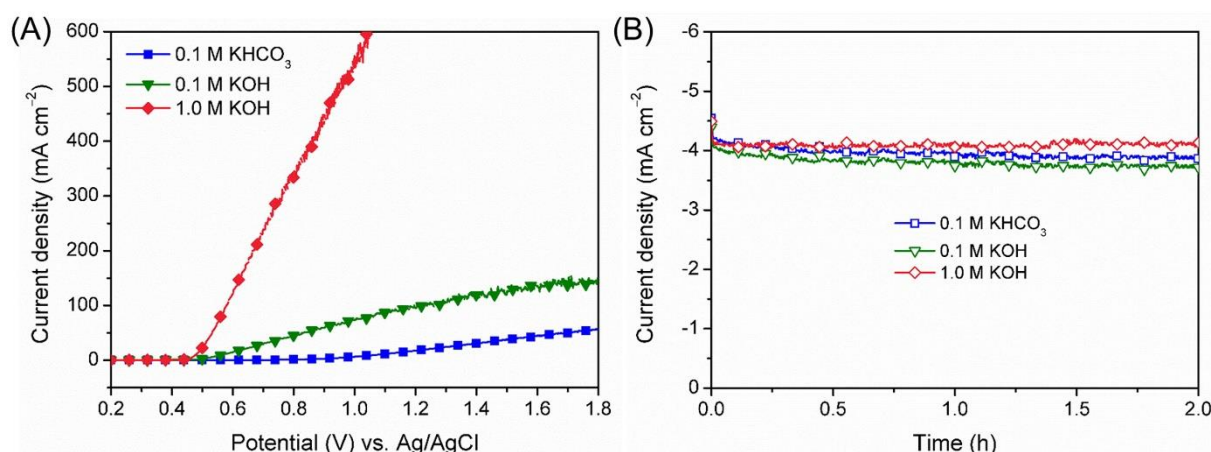


Figure 6. A, LSV curves of OER recorded on Ir/C modified GCE in CO₂-saturated 0.1 M KHCO₃ catholyte and three different anolytes (0.1 M KHCO₃, 0.1 M KOH or 1.0 M KOH) at 5 mV s⁻¹ (the counter electrode is r-Bi₂O₃/GCE). B, current density versus time during ERC using r-Bi₂O₃||Ir/C system in 0.1 M KHCO₃ catholyte and three different anolytes (0.1 M KHCO₃, 0.1 M KOH or 1.0 M KOH).

The differences between the KOH and KHCO₃ anolytes were studied for a system where the OER takes place at the anode, the following alkaline and acidic mediums, respectively:



For the KHCO₃ anolyte, HCO₃⁻ may react with the H⁺ generated in the OER (see Equation 5) following Equation 6:



The abovementioned suggestions were verified by quantitatively analyzing the concentration of the HCO₃⁻ solution in the anodic chamber before and after electrolysis. When the electrolytic charge

reached 50, 100, 150 or 200 C after a period potentiostatic electrolysis for the $r\text{-Bi}_2\text{O}_3 \parallel \text{Ir}/\text{C}$ system at a cell potential of 2.83 V by using KHCO_3 solution as the anolyte. The concentration of HCO_3^- in the anode chamber was obtained by titration with HCl solution and then, compared with the initial concentration before electrolysis. As shown in Figure 7, the residual concentration of HCO_3^- decreased gradually with the increase of electrolytic charge. When all the H^+ reacted with HCO_3^- , the residual HCO_3^- concentration in the anodic chamber, at the end of electrolysis, could be estimated. The abovementioned theoretical calculation results looked very close to the experimental data. Therefore, both KOH and KHCO_3 anolytes for ERC consumed anions, while excess K^+ entered the cathodic chamber through the Nafion 117 membrane.

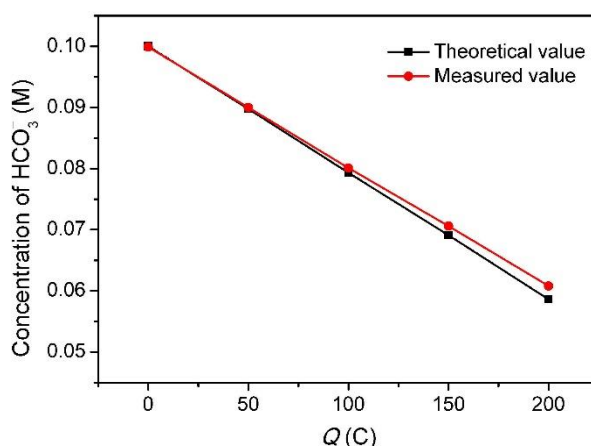


Figure 7. The theoretical and measured concentration of HCO_3^- in the anode compartment when the total passed charge is range from 0 to 200 C.

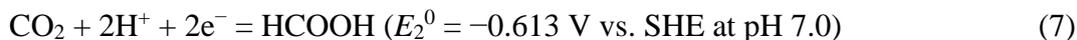
In contrast to the KHCO_3 anolyte, the KOH anolyte showed a similar functionality and a relatively lower energy efficiency. The KOH anolyte can be considered more suitable for the ECR to formate for the following three reasons, (i) in terms of actual energy consumption, the energy input for KOH anolyte is significantly lower than that of KHCO_3 anolyte because of the lower cell potential of the KOH anolyte; (ii) from the perspective of cost, using KOH is more economical than KHCO_3 ; and (iii) HCO_3^- in the KHCO_3 anolyte releases CO_2 (see Equation 6), which is an undesirable side reaction.

3.4 Mini review on the calculation of the energy efficiency

Estimates of energy efficiencies have not been consistent across literature [12, 18, 34]. Some consider 1.43 V as $|E^0|$ [5, 23, 35], in which E^0 has been obtained by subtracting the standard anode potential (0.813 V) from the standard cathode potential (-0.613 V) for neutral pH values of both the anolyte and catholyte. However, this may not be a practical assumption since the electrode potential tends to change as the pH value in the electrolyte changes. When the anolyte is 0.1 M KHCO_3 (pH=8.5), the main anode reaction shown in Equation 5 occurs, and the standard anode potential should be 0.727 V according to the Nernst equation. When the anolyte is 0.1 M KOH (pH=13) or 1 M KOH (pH=14),

the main anode reaction shown in Equation 4 occurs, and the standard anode potential should be 0.46 or 0.42 V, based on the Nernst equation.

The standard cathode potential has also not been calculated in a consistent way in studies reporting the ERC to formate. In most literature, the cathode reaction was taken to occur in neutral pH, as follows [34]:



At the neutral pH, the product from the ERC is formate (HCOO^-) instead of HCOOH . A more accurate cathode reaction could be that shown in Equation 3, thus, the value of $|E^0|$ would not be 1.43 V. The values of the actual $|E^0|$ and the corresponding energy efficiency (EE) in this work are given in Table 1, together with the energy efficiency ($EE^\#$) calculated with $|E^0|=1.43$ V. We can see that the $EE^\#$ for the ERC to formate can reach 65.9% using the $\text{r-Bi}_2\text{O}_3 \parallel \text{Ir/C}$ system in 1.0 M KOH anolyte. It is evident that the values of EE and $EE^\#$ can be significantly different. The value of $EE^\#$ is higher than that of EE , especially as the anolyte is changed from KHCO_3 solution to KOH solution. Therefore, energy efficiency must be carefully calculated to obtain useful data.

Table 1. Comparison of the traditional and actual values of the energy efficiency for the ERC to formate

Two-electrode system	Anolyte	Cell potential (V)	FE (%)	$EE^\#$ (%)	$ E^0 $ (V)	EE (%)
$\text{Sn} \parallel \text{Pt}$	0.1 M KHCO_3	3.85	73.0	27.1	1.157	21.9
$\text{r-Bi}_2\text{O}_3 \parallel \text{Pt}$	0.1 M KHCO_3	3.30	95.1	41.2	1.157	33.3
$\text{r-Bi}_2\text{O}_3 \parallel \text{Ir/C}$	0.1 M KHCO_3	2.83	95.3	48.1	1.157	39.0
	0.1 M KOH	2.31	94.8	58.7	0.89	36.5
	1 M KOH	2.06	95.0	65.9	0.83	38.2

4. CONCLUSIONS

A reduced Bi_2O_3 ($\text{r-Bi}_2\text{O}_3$) catalyst was prepared by the electrochemical reduction of the pre-synthesized Bi_2O_3 nanoparticles and used as a cathodic catalyst for the ERC to formate in a divided H-type electrolytic cell. When using Pt plate as the anode, the $\text{r-Bi}_2\text{O}_3$ cathodic catalyst with excellent ERC activity had a lower cell potential (3.30 V) and a higher energy efficiency (33.3%), compared to the Sn foil. The energy efficiency was further increased to 39% by using Ir/C, with excellent OER activity, as the anodic catalyst, with a low cell potential of 2.83 V. When the KHCO_3 anolyte was replaced by the KOH anolyte, the cell potential reduced and further declined as the KOH concentration increased. The cell potential and energy efficiency of the ERC to formate in the $\text{r-Bi}_2\text{O}_3 \parallel \text{Ir/C}$ system reached 2.06 V and 38.2% in 0.1 M KHCO_3 catholyte and 1.0 M KOH anolyte. In contrast to the KHCO_3 anolyte, the KOH anolyte was found to be more suitable for the ECR to formate.

ACKNOWLEDGEMENTS

This study was supported by the National Natural Science Foundation of China (grant numbers 21906142, 21876144, and 21603184).

References

1. C. Xia, P. Zhu, Q. Jiang, Y. Pan, W.T. Liang, E. Stavitsk, H.N. Alshareef, H.T. Wang, *Nat. Energy*, 4 (2019) 776.
2. S. Zhang, Q. Fan, R. Xia, T.J. Meyer, *Acc. Chem. Res.*, 53 (2020) 255.
3. S. Gao, Y. Lin, X.C. Jiao, Y.F. Sun, Q.Q. Luo, W.H. Zhang, D.Q. Li, J.L. Yang, Y. Xie, *Nature*, 529 (2016) 68.
4. T.B. Yuan, Z. Hu, Y.X. Zhao, J.J. Fang, J. Lv, Q.H. Zhang, Z.B. Zhuang, L. Gu, S. Hu, *Nano Lett.*, 20 (2020) 2916.
5. R. Zhang, W.X. Lv, G.H. Li, M.A. Mezaal, L.X. Lei, *RSC Adv.*, 5 (2015) 68662.
6. D. Li, J. Wu, T.T. Liu, J. Liu, Z.Y. Yan, L. Zhen, Y.J. Feng, *Chem. Eng. J.*, 375 (2019) 122024.
7. W.X. Lv, J. Zhou, J.J. Bei, R. Zhang, L. Wang, Q. Xu, W. Wang, *Appl. Surf. Sci.*, 393 (2017) 191.
8. W.X. Lv, J.J. Bei, R. Zhang, W.J. Wang, F.Y. Kong, L. Wang, W. Wang, *ACS omega*, 2 (2017) 2561.
9. R. Zhang, W.X. Lv, L.X. Lei, *Appl. Surf. Sci.*, 356 (2015) 24.
10. S. Gao, X.C. Jiao, Z.T. Sun, W.H. Zhang, Y.F. Sun, C.M. Wang, Q.T. Hu, X.L. Zu, F. Yang, S.Y. Yang, L. Liang, J. Wu, Y. Xie, *Angew. Chem. Int. Ed.*, 55 (2016) 698.
11. X.Q. Min, M.W. Kanan, *J. Am. Chem. Soc.*, 137 (2015) 4701.
12. N. Han, Y. Wang, H. Yang, J. Deng, J.H. Wu, Y.F. Li, Y.G. Li, *Nat. Commun.*, 9 (2018) 1320.
13. Q.Q. Li, X.R. Zhang, X.D. Zhou, Q.Y. Li, H.Q. Wang, J. Yi, Y.Y. Liu, J.J. Zhang, *J. CO₂ Util.*, 37 (2020) 106.
14. G. Díaz-Sainz, M. Alvarez-Guerra, J. Solla-Gullón, L. García-Cruz, V. Montiel, A. Irabien, *J. CO₂ Util.*, 34 (2019) 12.
15. X. Zhang, X.F. Hou, Q. Zhang, Y.X. Cai, Y.Y. Liu, J.L. Qiao, *J. Catal.*, 365 (2018) 63.
16. Q.N. Wang, H. Dong, H.B. Yu, *J. Power Sources*, 271 (2014) 278.
17. Q.N. Wang, H. Dong, H.B. Yu, H. Yu, M.H. Liu, *RSC Adv.*, 5 (2015) 10346.
18. C.C. Zhao, J.L. Wang, *Chem. Eng. J.*, 293 (2016) 161.
19. W.X. Lv, S.X. Liu, R. Zhang, W.J. Wang, Z.X. Wang, L. Wang, W. Wang, *J. Mater. Sci.*, 53 (2018) 4939.
20. Y.F. Zhou, Z.X. Wang, Z.Y. Pan, L. Liu, J.Y. Xi, X.L. Luo, Y. Shen, *Adv. Mater.*, 31 (2019) 1806769.
21. H.R. Yu, N. Danilovic, Y. Wang, W. Willis, A. Poozhikunnath, L. Bonville, C. Capuano, K. Ayers, R. Maric, *Appl. Catal. B: Environ.*, 239 (2018) 133.
22. R. Zhang, W.X. Lv, G.H. Li, M.A. Mezaal, X.J. Li, L.X. Lei, *J. Power Sources*, 272 (2014) 303.
23. C.C. Zhao, J.L. Wang, J.B. Goodenough, *Electrochem. Commun.*, 65 (2016) 9.
24. Q.N. Wang, H. Dong, H. Yu, H.B. Yu, *J. Power Sources*, 279 (2015) 1.
25. Q.N. Wang, H. Dong, H.B. Yu, *RSC Adv.*, 4 (2014) 59970.
26. J.J. Wu, F.G. Risalvato, F.S. Ke, P.J. Pellechia, X.D. Zhou, *J. Electrochem. Soc.*, 159 (2012) F353.
27. S.R. Narayanan, B. Haines, J. Soler, T.I. Valdez, *J. Electrochem. Soc.*, 158 (2011) A167.
28. G.K.S. Prakash, F.A. Viva, G.A. Olah, *J. Power Sources*, 223 (2013) 68.
29. W.X. Lv, R. Zhang, P.R. Gao, L.X. Lei, *J. Power Sources*, 253 (2014) 276.
30. Y. Hori, Modern Aspects of Electrochemistry, in: C.G. Vayenas, R.E. White, M.E. Gamboa-Aldeco (Eds.), Springer, (2008) New York, United States.
31. Y.Z. Fan, X. Cheng, *J. Electrochem. Soc.*, 163 (2016) E209.
32. A.P. Wu, Y. Xie, H. Ma, C.G. Tian, Y. Gu, H.J. Yan, X.M. Zhang, G.Y. Yang, H.G. Fu, *Nano Energy*, 44 (2018) 353.
33. W.C. Ma, S.J. Xie, X.G. Zhang, F.F. Sun, J.C. Kang, Z. Jiang, Q.H. Zhang, D.Y. Wu, Y. Wang, *Nat.*

Commun., 10 (2019) 892.

34. J.J. Wu, F.G. Risalvato, P.P. Sharma, P.J. Pellechia, F.S. Ke, X.D. Zhou, *J. Electrochem. Soc.*, 160 (2013) F953.

35. D.T. Whipple, E.C. Finke, P.J.A. Kenis, *Electrochem. Solid-State Lett.*, 13 (2010) B109.

© 2021 The Authors. Published by ESG (www.electrochemsci.org). This article is an open access article distributed under the terms and conditions of the Creative Commons Attribution license (<http://creativecommons.org/licenses/by/4.0/>).